Published in final edited form as:

Circulation. 2021 February 23; 143(8): 805–820. doi:10.1161/CIRCULATIONAHA.120.048121.

Cardiac pressure overload decreases ETV1 expression in the left atrium, contributing to atrial electrical and structural remodeling

Naoko Yamaguchi, MD PhD[1,*], **Junhua Xiao, MD PhD**[1,*], **Deven Narke, MS**[1], **Devin Shaheen, BS**[1], **Xianming Lin, PhD**[1], **Erik Offerman, MD**[1], **Alireza Khodadadi-Jamayran, PhD**[2], **Akshay Shekhar, PhD**[3], **Alex Choy, MD**[4], **Sojin Y. Wass, MD**[5], **David R. Van Wagoner, PhD**[5], **Mina K. Chung, MD**[5], **David S. Park, MD PhD**[1]

[1]The Leon H. Charney Division of Cardiology, New York University Grossman School of Medicine, 435 E 30th Street, Science Building 723, New York, New York 10016, USA

[2]NYU Applied Bioinformatics Labs, New York University Grossman School of Medicine, 227 E 30th Street, TRB-745, New York, New York 10016, USA

[3]Regeneron Pharmaceuticals, Inc. Biotechnology, 777 Old Saw Mill River Road, Tarrytown, NY, 10591 USA

[4]Icahn Medical Institute at Mount Sinai, 1 Gustave L. Levy Place, New York, NY 10029, USA

[5]Department of Cardiovascular & Metabolic Sciences; Department of Cardiovascular Medicine, Cleveland Clinic, 9500 Euclid Avenue, Cleveland, OH 44195, USA

Abstract

Background: Elevated intracardiac pressure due to heart failure induces electrical and structural remodeling in the left atrium (LA) that begets atrial myopathy and arrhythmias. The underlying molecular pathways that drive atrial remodeling during cardiac pressure overload are poorly defined. The purpose of this study is to characterize the response of the ETV1 signaling axis in the LA during cardiac pressure overload in humans and mouse models and explore the role of ETV1 in atrial electrical and structural remodeling.

Methods: We performed gene expression profiling in 265 left atrial samples from patients who underwent cardiac surgery. Comparative gene expression profiling was performed between two murine models of cardiac pressure overload, transverse aortic constriction (TAC) banding and Angiotensin II (AngII) infusion, and a genetic model of *Etv1* cardiomyocyte-selective knockout ($Etv1^{f/f}Mlc2a^{Cre/+}$).

Results: Using the Cleveland Clinic biobank of human LA specimens, we found that *ETV1* expression is decreased in patients with reduced ejection fraction. Consistent with its role as an important mediator of the Neuregulin-1 (NRG1) signaling pathway and activator of rapid conduction gene programming, we identified a direct correlation between *ETV1* expression level

Address for Correspondence: David S. Park, MD PhD, 435 E 30th Street, Science Building 711, New York, NY 10016, drdavidpark@gmail.com, Phone: 212-263-4131.
*These authors contributed equally to this work.

Disclosures
None.

and *NRG1, ERBB4, SCN5A*, and *GJA5* levels in human LA samples. In a similar fashion to heart failure patients, we showed that left atrial ETV1 expression is downregulated at the RNA and protein levels in murine pressure overload models. Comparative analysis of LA RNA-seq datasets from TAC and AngII treated mice showed a high Pearson correlation, reflecting a highly ordered process by which the LA undergoes electrical and structural remodeling. Cardiac pressure overload produced a consistent downregulation of *ErbB4, Etv1, Scn5a*, and *Gja5* and upregulation of profibrotic gene programming, which includes *Tgfbr1/2, Igf1*, and numerous collagen genes. $Etv1^{f/f}Mlc2a^{Cre/+}$ mice displayed atrial conduction disease and arrhythmias. Correspondingly, the LA from $Etv1^{f/f}Mlc2a^{Cre/+}$ mice showed downregulation of rapid conduction genes and upregulation of profibrotic gene programming, whereas analysis of a gain-of-function ETV1 RNA-seq dataset from neonatal rat ventricular myocytes transduced with *Etv1* showed reciprocal changes.

Conclusions: ETV1 is downregulated in the LA during cardiac pressure overload, contributing to both electrical and structural remodeling.

Keywords

heart failure; pressure overload; atrial remodeling; cardiac conduction disease; transcriptional biology; atrial fibrillation; ETV1/Er81

Introduction

Heart failure (HF), which affects more than 5 million Americans and approximately 23 million patients globally[1], is a complex clinical syndrome caused by functional or structural defects of the cardiovascular system that result in elevated intracardiac pressure[2]. Chronic pressure overload induces a series of electrical and structural changes, known as remodeling, in the heart that allow arrhythmias to initiate and perpetuate. The left atrium (LA) is particularly vulnerable to the remodeling process when exposed to pressure overload. Biophysical changes in the LA give rise to slow conduction and increased atrial ectopy, while increased fibrosis synergizes with electrophysiological changes to create the substrate for reentrant arrhythmias, such as atrial tachycardia, atrial flutter (AFL), and atrial fibrillation (AF). AFL and AF are highly prevalent in the HF population, increasing stroke risk, morbidity, and mortality. Defining the molecular pathways that drive adverse remodeling in the LA during cardiac pressure overload is essential for the development of therapies that can halt or reverse the remodeling process.

Atrial myocardium has rapid conduction features due to enriched expression of the pore forming subunit of the cardiac sodium channel, $Na_V1.5$ (encoded by *Scn5a*) and the high conductance gap junction protein, Cx40 (encoded by *Gja5*). $Na_V1.5$ mediates the influx of the fast sodium current (I_{Na}), which is the principal determinant of membrane excitability and conduction in atrial myocytes. Cx40 is a major contributor to passive conductance in the atrial myocardium that ensures rapid impulse propagation. The remodeled atrium exhibits reduced conduction velocity as a result of decreased I_{Na}[3], diminished expression of Cx40[4, 5], and increased atrial fibrosis[6], which impairs conduction by disrupting muscle fiber continuity. Together, these electrical and structural alterations in the LA create

the substrate that sustains atrial rhythm abnormalities. What remains unresolved is how upstream signaling and transcriptional pathways orchestrate the remodeling process.

We recently discovered that the Neuregulin-1 (NRG1)/ Erb-B2 Receptor Tyrosine Kinase 4 (ErbB4)/ E twenty-six variant 1 (ETV1) signaling axis is a key determinant of rapid conduction gene programming in the atria and His-Purkinje system (HPS)[7, 8]. NRG1 secreted from endocardial cells binds to its cognate receptor ErbB4 in atrial and Purkinje myocytes, turning on the expression and activity of transcription factor ETV1, which upregulates the expression of *Scn5a* and *Gja5*[7, 8]. *Etv1* deficient mice exhibit conduction disease in the atria and HPS due to a reduction in *Scn5a* and *Gja5*, in addition to hypomorphism of the HPS. Moreover, loss of ETV1 disrupts the normal enrichment and biophysical heterogeneity of I_{Na} present in atrial and Purkinje myocytes[7, 8].

Based on the importance of ETV1 in establishing rapid conduction physiology in atrial myocytes, we hypothesized that alterations in the ETV1 signaling axis would play an important role in remodeling the LA during cardiac pressure overload. Our results show that ETV1 expression is significantly down-regulated in the LA from patients with reduced ejection fraction and from two pressure overload mouse models. Using both loss-of-function and gain-of-function models, we demonstrate an important role for the ErbB4/ETV1 signaling axis in both electrical and structural remodeling in the LA.

Materials and Methods

A detailed description of all materials and methods including RNA sequencing (RNA-seq) data preparation and analyses, electrocardiography (ECG), echocardiography, and Western blot is provided in the online Data Supplement. Genetically modified animals are available from the corresponding author on reasonable request.

Experimental animals and study design

All animal experimental procedures were approved by the Institutional Animal Care and Use Committee of New York University Grossman School of Medicine, protocol #IA16-01599 and the animals received humane care in accordance with the *Guide for the Care and Use of Laboratory Animals* by National Institutes of Health. C57BL/6J mice (8–10-week-old males) were purchased from The Jackson Laboratory (Farmington, CT). $Etv1^{f/f}$ mice (a generous gift from Dr. Silvia Arber, University of Basel, Switzerland), were crossed with $Mlc2a^{Cre/+}$ mice[9] ($Myl7^{tm1(cre)Krc}$, a generous gift from Dr. Kenneth R. Chien, Karolinska Institutet, Stockholm, Sweden and kindly shared by Dr. Xu Peng, Texas A&M University, TX, USA) in a C57BL/6J background. $Etv1^{f/f}Mlc2a^{Cre/+}$ were used as *Etv1* cardiomyocyte knockout mice, and littermate $Etv1^{f/f}$ mice as control. $Etv1^{nlz/+}$ [8, 10] was a generous gift from Dr. Silvia Arber (University of Basel, Switzerland).

Mouse model of pressure overload by Angiotensin II (AngII) infusion

Mini-osmotic pumps (Alzet model 2004, DURECT Corporation, Cupertino, CA) were implanted subcutaneously in the interscapular region[11] in six $Etv1^{nlz/+}$ mice and twenty six C57BL/6J mice under inhaled 2 % isoflurane. AngII solution was continuously infused

at the rate of 2 mg/kg/day for 2 weeks for the *Etv1*$^{nlz/+}$ and C57BL/6J mice. Saline was given to control mice (four *Etv1*$^{nlz/+}$ mice or thirteen C57BL/6J mice).

Mouse model of pressure overload by transverse aortic constriction (TAC) procedure

Constriction of the transverse thoracic aorta[12] was performed on six *Etv1*$^{nlz/+}$ and thirty five male C57BL/6J mice. Anesthesia was maintained with 1–2 % isoflurane by endotracheal intubation. Buprenorphine was given subcutaneously at 0.1 mg/kg dose every 12 hours till 72-hours post-procedure. After a midline sternotomy, 7-0 silk suture was tightened against a 27-gauge needle placed adjacent to the aorta distal to the brachiocephalic artery. Sternotomy and skin closure were performed using 6-0 polypropylene suture. Twenty sham mice underwent aforementioned procedure but without TAC.

Whole-mount staining & imaging for β-galactosidase activity

Hearts were perfusion-fixed with 2 % paraformaldehyde and stained with solution containing 5 bromo-4-chloro-3-indolyl-β-d-galactopyranoside, as previously described[8]. Bright-field images of hearts were taken using the Zeiss Discovery V8 microscope equipped with a Zeiss AxioCam Color camera interfaced with Zeiss Zen 2012 software (ZEISS, Oberkochen, Germany).

Human subjects and RNA-seq

As previously reported by Hsu, et al.[13], polyA+RNA sequencing was performed on left atrial appendage (LAA) tissues from a total of 265 subjects (235 subjects of European descent, and 30 of African descent, mean age 60±12 years, 181 males). Clinical characteristics of the patients are summarized in Table 1. All surgical patients provided informed consent for research use of discarded atrial tissue in a process approved by the Cleveland Clinic Institutional Review Board (IRB). The IRB approved the studies included in this report (#2018-1501, D.V.W). Library generation for RNA-seq was done at the University of Chicago Genomics Facility. Gene read counts are available in the Gene Expression Omnibus database (GSE69890).

Rodent RNA-seq

Total RNA extracted from the left atrial tissue of TAC banded and sham mice were used for RNA-seq. For detailed methods for rodent RNA sample preparation, sequencing, and analysis, see online supplementary materials and methods. RNA-seq data[14] from *Etv1*^{MLCCre} (presented here as *Etv1*$^{f/f}$*Mlc2a*$^{Cre/+}$) and pressure overload model mice with AngII infusion for 2 weeks were reanalyzed for this study. Details about the genetically modified mouse model and sample preparation are described in Rommel, et al.[14] RNA-seq data from ETV1-transduced neonatal rat ventricular myocytes (NRVMs) were reanalyzed from our published data for this study[7].

Whole-cell I_{Na} recordings

Left atrial myocytes were isolated from *Etv1*$^{f/f}$*Mlc2a*$^{Cre/+}$ or littermate control (*Etv1*$^{f/f}$) hearts that were Langendorff perfused and enzymatically digested for I_{Na} recordings as previously described[7, 8]. All recordings were obtained three times to verify reproducible

recordings and within 15 minutes after establishing whole-cell configuration at room temperature with voltage step protocols using an Axon multiclamp 700B Amplifier coupled to a pClamp system (v10.2, Axon Instruments).

Statistical Analysis

Statistical analyses were conducted using JMP 11 (SAS Institute, Cary, NC) for human RNA-seq data and Graph Pad Prism 8 (GraphPad Software, San Diego, CA) for other experiments. Simple linear regression analyses were performed to examine the correlation between *ETV1* and left ventricular ejection fraction (LVEF), *NRG1, ERBB4, SCN5A*, and *GJA5*. One-way analysis of variance was used for the comparison between *ETV1* and AF diagnosis/subtype. For quantitative data, Shapiro–Wilk test was used to test a normal distribution. A two-tailed unpaired Student's *t*-test was used for Western blot and cardiac physiological assessment, I_{Na} measurements, and fibrosis assessment unless otherwise mentioned in the figure legend. Differences were considered to be statistically significant at $P < 0.05$.

Data availability

The mouse lines will be made publicly available through a mouse repository. RNA-seq data has been deposited with the NCBI; for AngII mouse model and $Etv1^{MLCCre}$ ($Etv1^{f/f}$ $Mlc2a^{Cre/+}$) mice, under the BioProject ID: PRJNA470522; for NRVMs, under the Gene Expression Omnibus (GEO) accession number: GSE115061; for human in the GSE69890.

Results

ETV1 is downregulated in human heart disease

To study the role of ETV1 in human heart disease, we analyzed a left atrial RNA-seq database containing 265 patient samples (251 patients who underwent heart surgery and 14 heart donors unmatched for heart transplant) from the Cleveland Clinic. Patient characteristics are presented in Table 1. Of the 251 study subjects, 184 patients (73 %) had New York Heart Association (NYHA) functional classification II or higher, the mean LVEF was 51±12 %, and 213 patients had a diagnosis of AF (85 %). The analysis showed a significant association between reduced LVEF with lower left atrial *ETV1* expression (Figure 1A). We also examined the relationship between *ETV1* expression levels and AF diagnosis/active rhythm at the time of cardiac surgery. There was no significant association between *ETV1* expression in the LA and AF diagnosis ($R = 0.05$, $P = 0.78$; Figure 1B) or AF subtype (Figure I in the Supplement), which differs from a previous report that suggested an increase in *ETV1* expression with AF in a very small sample size[14].

We previously showed that ETV1 is regulated at the transcriptional and post-translational levels by the NRG1/ERBB4/mitogen-activated protein kinase (MAPK) signaling pathway in the rodent heart[8]. We also showed that ETV1 is sufficient to turn on *SCN5A* and *GJA5* in rodent and human cardiomyocytes[7, 8]. Based on these findings, we next examined if *ETV1* exhibits a conserved relationship with the ERBB4 signaling pathway and rapid conduction genes in the human LA. *ETV1* levels directly correlate with *NRG1, ERBB4, SCN5A*, and

GJA5 (Figure 1C). These results support a conserved role for the NRG1/ERBB4/ETV1 signaling pathway in regulating rapid conduction physiology in the human LA.

Downregulation of *Etv1*$^{nlz/+}$ reporter gene expression in cardiac pressure overload models

Etv1 is robustly expressed in the atria and HPS as delineated by the *Etv1*$^{nlz/+}$ reporter mouse[8]. To assess whether *Etv1* expression levels are altered in the LA during cardiac pressure overload, we performed TAC banding in wildtype (WT) C57BL/6J and *Etv1*$^{nlz/+}$ reporter mice. TAC banding surgically elevates intracardiac pressure in the left ventricle (LV) and LA by creating a fixed afterload obstruction, which results in left atrial enlargement (Figure IIA, B in the Supplement), concentric LV hypertrophy, and reduced systolic function (Figure IIB in the Supplement). ECG assessment demonstrated significantly prolonged P wave duration (18.4±1.0 ms, n = 8 vs.17.2±0.6 ms, n = 5, TAC vs. sham, P = 0.0333), QRS interval duration (14.2±3.5 ms, n = 8 vs.10.7±0.6 ms, n = 5, TAC vs. sham, P = 0.0109) and corrected QT interval (QTc) (50.4±17.6 ms, n = 8 vs.36.8±1.4 ms, n = 5, TAC vs. sham, P = 0.0031) in TAC banded mice compared to sham mice (Figure IIC in the Supplement). After two weeks of TAC banding, *Etv1-nlz* reporter gene expression was significantly reduced in the LA with little to no change in the right atrium (RA) (Figure 2A, B).

We next treated WT C57BL/6J and *Etv1*$^{nlz/+}$ reporter mice with AngII, which induces high systemic blood pressure. AngII infusion caused left atrial enlargement and left ventricular hypertrophy (Figure IIIA, B in the Supplement). Compared to control mice, AngII treated mice showed significantly increased heart rate (545±44 beats/min, n = 8 vs. 488±16 beats/min, AngII vs. control, n = 8, P = 0.0044), P wave duration (18.7±0.9 ms, n = 8 vs. 17.4±0.3 ms, n = 8, AngII vs. control, P = 0.0015), QRS interval duration (11.6±0.8 ms, n = 8 vs.10.1±0.4 ms, n = 8, AngII vs. control, P = 0.0014)) and QTc (41.9±2.7 ms, n = 8 vs. 36.2±2.3 ms, n = 8, AngII vs. control, P = 0.0004) (Figure IIIC in the Supplement). Similar to TAC banded mice, AngII treatment reduced *Etv1-nlz* reporter gene expression in the LA, whereas no change was evident in vehicle control treated mice (Figure 2C). AngII treatment showed reduced expression of *Etv1-nlz* reporter gene expression in the RA but to a lesser extent than in the LA (Figure 2C, D).

Cardiac pressure overload with TAC or AngII induces a highly ordered remodeling process in the LA

We next performed comparative, differential gene expression analysis of left atrial RNA-seq datasets generated from TAC banded and AngII[14] treated mice. The RNA-seq datasets showed considerable overlap in gene expression changes between the two model systems. Of the 4126 genes that are differentially expressed with AngII treatment, 3364 genes overlap with TAC banding (Figure 3A). Notably, the 3364 overlapping genes from both model systems decrease (1694 genes) and increase (1670 genes) in a highly similar manner (Pearson correlation R = 0.88, P < 2.2e–16) (Figure 3B).

Differentially expressed genes that were significantly downregulated and upregulated in both pressure overload models were then analyzed using the Kyoto Encyclopedia of Genes and Genomes (KEGG) pathway analysis. The biological processes that are

significantly downregulated are involved in neuronal pathways (Parkinson's, Alzheimer's, and Huntington's), oxidative phosphorylation pathways, and metabolic processes (TCA cycle, Fatty acid metabolism, Glycolysis/Gluconeogenesis, Amino Acid biosynthesis) (Table I in the Supplement). The signaling pathways that are significantly downregulated are involved in adrenergic signaling, cGMP-PKG signaling, cAMP signaling, calcium signaling, ErbB signaling, and MAPK signaling pathways (Figure 3C). Network analysis of the downregulated signaling pathways reveal interactions between pathways involved in sodium channel regulation (Adrenergic signaling: *Scn5a*[15], *Scn4b*[16] and MAPK signaling: *Fgf12*[17], *Fgf13*[18, 19]), calcium handling[20] (*Cacna1H, Cacna2D3, Cacna1D, Cacna1S, CacnB2, Pln, Ryr2*), and the ErbB4[8] signaling pathway (Figure IVA in the Supplement).

The biological processes that are most significantly upregulated in the LA of pressure overload models are related to hypertrophic and dilated cardiomyopathy as well as pathways involved in collagen deposition, such as extracellular matrix (ECM), focal adhesion, protein digestion and absorption, and cancer pathways (Table II in the Supplement). Notably, the signaling pathways that are significantly upregulated are involved in PI3K-Akt signaling, p53 signaling, Rap1 signaling, Ras signaling, HIF-1 signaling and TGF-β signaling pathways (Figure 3D). Interestingly, many of these pathways have in common the upregulation of insulin-like growth factor I (*Igf1*). As shown in the network plot (Figure IVB in the Supplement) and in Table III in the Supplement, *Igf1* links hypertrophic and dilated cardiomyopathy with profibrotic biological processes (focal adhesion, pathways in cancer) and important signaling pathways (PI3K-Akt signaling, p53 signaling, Rap1 signaling, Ras signaling, and HIF-1 signaling pathways). The central role of IGF1 in left atrial pressure overload is particularly interesting given a recent study by Wang et al.[21] that found that IGF1 upregulation is an important determinant of atrial fibrosis through regulation of PI3K-Akt signaling in a rat atrial tachy-paced model.

Volcano plots displaying the variance in differentially expressed transcripts from TAC banded and AngII infused cardiac pressure overload models are shown in Figure 3E and 3F, respectively. *Etv1, ErbB4, Scn5a*, and *Gja5* were significantly downregulated in both models, whereas TGF-β receptors 1 and 2 (*Tgfbr1* and *Tgfbr2*), *Igf1*, and numerous collagen genes were significantly upregulated.

Prior work by Rommel et al.[14] suggested that ETV1 increases in a small sampling of human RA biopsies in patients with AF. To address the differences between our findings and the previous work, we tested several antibodies for their ability to detect ETV1 protein in the heart and cerebellum of germline *Etv1* knockout ($Etv1^{nlz/nlz}$) vs WT littermate controls. As shown in Figure V in the Supplement, an anti-ETV1 (ER81, ab184120) antibody from Abcam was confirmed to detect ETV1 in the heart and brain. ETV1 is expressed in WT atria but not in WT LV apex or germline *Etv1* knockout atria. The antibody that was used by Rommel et al. shows no specific detection of ETV1 protein in the heart or brain samples.

Using the Abcam anti-ETV1 (ab184120) antibody, we showed that ETV1 is significantly reduced in the LA of TAC banded mice (Figure 4A, B), whereas RA ETV1 levels were unchanged (Figure VI in the Supplement). Protein levels of ErbB4 and $Na_V1.5$ were also significantly downregulated, while TGFBR2 was significantly upregulated in the LA of

TAC banded mice. To quantify the burden of fibrosis in the LA of TAC banded hearts, histological analysis was performed on Masson's trichrome stained sections using ImageJ (NIH, Bethesda, MD). The left atrial sections from TAC banded hearts showed increased fibrosis compared to sham hearts (Figure 4C). Similar to the TAC banded model, the LA samples from AngII treated mice showed significant decrease in ETV1, ERBB4, and $Na_V1.5$, and increase in TGFBR2 and left atrial fibrosis (Figure 4D–F). Therefore, cardiac pressure overload alters left atrial transcriptional programming in a highly ordered process that includes a downregulation of the ErbB4/ETV1 signaling axis.

Etv1 loss-of-function contributes to electrical and structural remodeling during cardiac pressure overload

To assess the contribution of *Etv1* loss-of-function to the atrial remodeling process, we generated an *Etv1* cardiomyocyte knockout ($Etv1^{f/f}Mlc2a^{Cre/+}$) mouse model that selectively targets *Etv1* exon 11 for deletion (Figure 5A). Left atrial ETV1 expression is significantly reduced at the protein level (Figure 5B, C). Surface ECG was performed on sedated $Etv1^{f/f}Mlc2a^{Cre/+}$ and control ($Etv1^{f/f}$) mice at 8–12 weeks of age (Figure 5D). $Etv1^{f/f}Mlc2a^{Cre/+}$ mice had significantly longer P wave (18.5±0.9 ms, n = 13, vs. 17.6±0.8 ms, n = 17, $Etv1^{f/f}Mlc2a^{Cre/+}$ vs. $Etv1^{f/f}$, P = 0.0049) and QRS wave durations (11.6±0.7 ms, n = 13, vs. 10.8±0.8 ms, n = 17, $Etv1^{f/f}Mlc2a^{Cre/+}$ vs. $Etv1^{f/f}$, P = 0.0056) than those observed in littermate controls. PR interval was also longer in $Etv1^{f/f}Mlc2a^{Cre/+}$ mice than in $Etv1^{f/f}$ mice. Figure 5E shows representative ECG traces from $Etv1^{f/f}Mlc2a^{Cre/+}$ mice showing atrial and ventricular arrhythmias. None of the $Etv1^{f/f}$ mice showed arrhythmia episodes. Table IV in the Supplement summarizes ECG rhythm assessment of $Etv1^{f/f}Mlc2a^{Cre/+}$, TAC banded and AngII infused models. While $Etv1^{f/f}Mlc2a^{Cre/+}$ mice demonstrated cardiac conduction abnormalities and arrhythmias, they showed no gross structural or functional changes on echocardiographic assessment compared to $Etv1^{f/f}$ mice (Figure VII in the Supplement).

To explore the molecular mechanisms underlying the observed electrophysiological defects in $Etv1^{f/f}Mlc2a^{Cre/+}$ mice, we used a left atrial, cardiomyocyte-purified, RNA-seq list from a previous report using the same *Etv1*-deficient ($Etv1^{f/f}Mlc2a^{Cre/+}$) mouse model[14], which demonstrated efficient knockout of exon 11 at the transcript level (data not shown). We performed principal-component analysis and Euclidean distance analysis on the 3 models to assess the robustness of the data (Figure VIII in the Supplement). The analysis of the $Etv1^{f/f}Mlc2a^{Cre/+}$ LA dataset revealed 495 differentially expressed genes, of which 433 genes overlapped with TAC banded and/or AngII treated models. Of these 433 genes, 281 overlapped with $Etv1^{f/f}Mlc2a^{Cre/+}$ and both pressure overload models (Figure 6A). The expression pattern of the 281 differentially expressed genes was notable for the high degree of similarity between all three model systems (Figure 6B). KEGG analysis of the 281 overlapping genes revealed a downregulation of adrenergic signaling, MAPK signaling, ErbB signaling, and calcium signaling pathways (Figure 6C). Specific genes that were downregulated included *ErbB4, Etv1, Scn5a*, and *Gja5* (Figure6D, E). Upregulated pathways included the PI3K-Akt pathway as well as numerous pathways with significant collagen gene enrichment, such as ECM-receptor interaction, focal adhesion, proteoglycans in cancer, and protein digestion and absorption pathways (Figure 6C). Specific genes that

were upregulated include *Tgfbr1, Tgfbr2, Igf1*, and numerous collagen genes (Figure 6D, E). Importantly, adenoviral-mediated overexpression of ETV1 in neonatal rat ventricular myocytes (NRVMs)[7] showed a reciprocal relationship, with an upregulation of fast conduction genes and a downregulation of *Tgfbr1, Tgfbr2, Igf1*, and collagen genes (Figure 6F).

We next validated these findings at the protein level using immunoblot assay from the LA of $Etv1^{f/f}Mlc2a^{Cre/+}$ mice (Figure 7A, B). ERBB4, $Na_V1.5$, and TGFBR2 showed similar changes in accordance with the RNA-seq result. Similar to the two pressure overload models, $Etv1^{f/f}Mlc2a^{Cre/+}$ left atria showed increased fibrosis compared to $Etv1^{f/f}$ littermate controls at 16–20 weeks of age (Figure 7C). Together, these findings support the hypothesis that the downregulation of ETV1 contributes to both electrical and structural remodeling in the LA during pressure overload.

Whole cell patch clamp was performed on left atrial myocytes from $Etv1^{f/f}Mlc2a^{Cre/+}$ and control ($Etv1^{f/f}$) mice to characterize I_{Na} (Figure 7D–G). The current density was significantly decreased in $Etv1^{f/f}Mlc2a^{Cre/+}$ compared to $Etv1^{f/f}$ (Figure 7D). At −40 mV, the peak I_{Na} density was decreased from −38.4±1.6 to −27.7±1.3 pA/pF in $Etv1^{f/f}Mlc2a^{Cre/+}$ ($P < 0.0001$ vs. $Etv1^{f/f}$). Although voltage dependence of steady-state activation did not significantly differ between the groups (Figure 7E), sodium channels in $Etv1^{f/f}Mlc2a^{Cre/+}$ underwent steady-state inactivation at less negative potentials compared to $Etv1^{f/f}$ (V1/2 inactivation: −86.2±1.1 mV in $Etv1^{f/f}Mlc2a^{Cre/+}$ vs. −90.9±1.1 mV in $Etv1^{f/f}$, $P = 0.004$, Figure 7F). Additionally, sodium channel recovery from inactivation was slower in $Etv1^{f/f}Mlc2a^{Cre/+}$ compared to $Etv1^{f/f}$ (2.9±0.2 ms in $Etv1^{f/f}Mlc2a^{Cre/+}$ vs. 1.9±0.2 ms in $Etv1^{f/f}$, $P = 0.003$, Figure 7G). Similar changes in the I_{Na} were noted in $Etv1^{f/f}$ $Mlc2a^{Cre/+}$ right atrial myocytes (data not shown), which corroborate our previous report[7] using the αMHC-Cre restricted *Etv1* knockout ($Etv1^{f/f}Myh6^{Cre/+}$) mouse model. These results emphasize the importance of ETV1 in maintaining the unique biophysical properties of I_{Na} in right and left atrial myocytes.

Discussion

This study provides evidence that cardiac pressure overload induces a highly ordered process of electrical and structural remodeling in the LA. Pressure overload in the LA leads to downregulation of the ErbB4/ETV1 signaling pathway that simultaneously decreases expression of rapid conduction genes and increases expression of pro-fibrotic genes. Our data provide a novel paradigm of atrial remodeling that suggests that electrical and structural changes are linked by common transcriptional pathways, such as ETV1, that are established during development.

This paradigm is quite plausible from a developmental perspective as regions of slow conduction, namely the sinoatrial and atrioventricular nodes, are immediately juxtaposed to rapidly conducting atrial myocardium, indicating that the transcriptional programs for slow or fast conduction are segregated into nearly binary terms in the atrial chambers. A distinguishing feature of the slowly conducting nodal regions is enhanced fibrosis, which serves two main functions: i) to maintain slow impulse propagation as a result

of poor cellular coupling and ii) to shield regions of slow conduction/automaticity from the hyperpolarizing influence of neighboring atrial myocytes. Taken from this perspective, the ability of ETV1 to drive rapid conduction gene expression while simultaneously repressing pro-fibrotic gene programs makes biological sense and reflects the efficiency of transcriptional programs.

Our approach to understanding left atrial electrical and structural remodeling from cardiac pressure overload was to focus our analysis on differentially expressed signaling pathways from two pressure overload models. By focusing our analysis on shared signaling pathways, we were able to identify higher order processes that govern the remodeling process. Using this approach, we identified that the major downregulated pathways include the ErbB signaling pathway, MAPK signaling pathway, adrenergic signaling in cardiomyocytes, and calcium signaling pathway. Combining the pressure overload models with the *Etv1*$^{f/f}$*Mlc2a*$^{Cre/+}$ model dataset shows that ETV1 links ErbB4/MAPK signaling with excitability and calcium handling genes. These data are consistent with our prior work showing that the ErbB4/MAPK signaling pathway regulates ETV1, which in turn drives the expression of rapid conduction genes, *Scn5a* and *Gja5*, in atrial myocytes[7, 8]. The ability of ETV1 to also regulate ErbB4 expression points to a feed forward mechanism, whereby ErbB4/ETV1 signaling reinforces itself to maintain a rapid conduction phenotype in atrial myocytes. Cardiac pressure overload interrupts this feedforward loop, decreasing both ETV1 and ErbB4 expression.

Major upregulated pathways that network together in the pressure overloaded LA include pathways involved in collagen deposition, such as ECM-receptor interaction, focal adhesion, PI3K-Akt signaling pathway and TGF-β signaling pathway. Combined analysis of the pressure overload models with the *Etv1*$^{f/f}$*Mlc2a*$^{Cre/+}$ RNA-seq dataset reveals how a loss of ETV1 coordinates the upregulation of pro-fibrotic gene programs through enhanced expression of *Tgfbr1, Tgfbr2, and Igf1*. Conversely, adenoviral-mediated overexpression of ETV1 in NRVMs reduced expression of *Tgfbr1, Tgfbr2, Igf1*, and numerous collagen genes, showing a repressive role for ETV1 on cardiomyocyte fibrosis pathways. TGF-β signaling has a well-accepted role in enhancing fibrotic pathways in numerous disease states, including cardiac diseases[22, 23]. Verrecchia et al.[24] demonstrated that TGF-β target genes include select collagen genes, including *Col1a1, Col1a2, Col3a1, Col5a2*, and *Col6a1*. It is notable that these select collagen genes as well as *Tgfbr1* and *Tgfbr2* are co-regulated by ETV1. The importance of IGF1 in atrial fibrosis was recently reported by Wang et al.[21] using a rat tachypacing model. Similar to our results, they reported a significant upregulation of IGF1 in the LA that corresponded with increased fibrosis. When IGF1 was down-regulated using shRNA-based gene silencing, the degree of atrial fibrosis with tachypacing was significantly attenuated. Taken together, our data suggests that ETV1 downregulation during cardiac pressure overload de-represses *Tgfbr1, Tgfbr2*, and *Igf1* expression in the LA, enhancing pro-fibrotic gene programming. Whether ETV1 regulates the expression of *Tgfbr1, Tgfbr2*, and *Igf1* through direct or indirect mechanisms is the subject of ongoing research.

Altered cardiac metabolism in the LA is notable in the pressure overload models. It has been reported that in hypertrophied and failing ventricular myocytes, cardiac substrate

utilization switches to a fetal-like metabolism, characterized by increased reliance on glucose and decreased fatty acid oxidation (FAO)[25]. Increased glucose utilization fuels aspartate production, which drives synthesis of nucleotides, RNA, and proteins that increase biomass needed for myocyte hypertrophy. Recent work by Ritterhoff et al.[26] shows that preservation of FAO by knocking down ACC2 (Acetyl-CoA carboxylase 2, encoded by *Acacb*) prevents glucose utilization needed for anabolic metabolism and cardiomyocyte hypertrophy. Our data suggest that atrial myocytes may undergo a similar switch in fuel metabolism, as evidenced by a decrease in fatty acid metabolic pathways. However, atrial myocytes do not undergo marked myocyte hypertrophy as seen in ventricular myocytes. It is worth noting that *Acacb* is downregulated in atrial myocytes in both pressure overload models and whether this prevents a more robust switch to glucose utilization and therefore, hypertrophic signaling, will need to be explored further. Moreover, whether altered metabolism in the pressure overloaded atrium contributes to the downregulation of Erbb4/ETV1 signaling will be investigated in future work.

A recent report from Rommel et al.[14] suggested that atrial ETV1 increases in human and mouse heart disease. In contrast, our data shows significantly lower levels of left atrial *ETV1* in patients with lower LVEF and in mouse models of cardiac pressure overload, and no significant relationship between *ETV1* level and AF in patients who had cardiac surgery for different etiologies. The discrepancy between our results and that of Rommel et al.[14] can be explained by several factors: i) the low number of patient samples used in the Rommel study (three right atrial samples for RNA analysis and nine right atrial samples used for protein analysis), ii) the use of right atrial instead of left atrial samples for human dataset, and iii) use of an antibody that we here show does not detect ETV1 protein on immunoblot analysis (Figure V in the Supplement). Reinforcing our findings from the human LA dataset that showed lower *ETV1* in HF patients, cardiac pressure overload using TAC banding or AngII infusion resulted in significant reduction of *Etv1-nlz* reporter gene expression in the LA. Intriguingly, comparative analysis of the AngII treated LA RNA-seq dataset generated by Rommel et al.[14] was in complete agreement with our TAC banded dataset, showing *Etv1* is downregulated in both model systems. Furthermore, a cardiac *Etv1* knockout ($Etv1^{f/f}Mlc2a^{Cre/+}$) left atrial, cardiomyocyte-purified, RNA-seq dataset[14] from the same group showed significant overlap and agreement with both pressure overload model systems, again in support of the hypothesis that cardiac pressure overload induces an *Etv1* loss-of-function gene profile. In our study, the $Etv1^{f/f}Mlc2a^{Cre/+}$ model showed cardiac conduction abnormalities and arrhythmias in both atria and ventricles, of which the conduction phenotype was previously reported with *Etv1* cardiac knockout by αMHC-Cre[7]. Lastly, Rommel et al. used an αMHC promoter driven *Etv1* transgenic ($Etv1^{\alpha MHC}$) mouse to support their gain-of-function hypothesis. The $Etv1^{\alpha MHC}$ transgenic mouse showed marked atrial and ventricular structural and functional abnormalities. ETV1 is a known oncogene that has been implicated in numerous cancers, including gastrointestinal stromal tumors[27], prostate cancer[28, 29], and breast cancer[30]. As αMHC has a transcript abundance of over 1 million copies compared to ~650 copies of *Etv1* in the LA, this is likely to have been highly oncogenic. No assessment or description was made of the proliferative state of atrial or ventricular myocytes in the $Etv1^{\alpha MHC}$ transgenic hearts.

Our results support the hypothesis that cardiac pressure overload induces an ETV1 loss-of-function state that contributes to adverse electrical and structural remodeling in the LA. The molecular pathways that result in ETV1 downregulation at the transcriptional level is an area of research that we are actively pursuing. As current pharmacotherapy for rhythm control of AF has been largely disappointing, novel therapies aimed at addressing the underlying remodeling process, such as ETV1 downregulation, will be of keen interest.

This study evaluated the gene profiling on total RNA extracted from LA tissue from two cardiac pressure overload models. It is known that there are multiple cardiac cell populations including cardiomyocytes, fibroblasts, endothelial cells, macrophages, and other leukocytes. Therefore, the individual cellular contributions to the global effect on gene expression changes will need to be delineated by single cell RNA-seq in the future. It is possible that a portion of the prolongation in QRS duration is contributed by *Mlc2a* haploinsufficiency or Cre transgene expression in the $Mlc2a^{Cre/+}$ mouse, as some non-significant QRS prolongation was noted in another model[31]. However, significant prolongation in P wave, PR interval, and QRS wave duration measured in the $Etv1^{f/f}Mlc2a^{Cre/+}$ mouse recapitulates the findings of *Etv1* germline knockout mice[8]. The biophysical changes in the I_{Na} seen in $Etv1^{f/f}Mlc2a^{Cre/+}$ LA and RA myocytes also recapitulates the findings of our previously published *Etv1* knockout models[7, 8].

Supplementary Material

Refer to Web version on PubMed Central for supplementary material.

Acknowledgments

The authors thank Mark Alu (Experimental Pathology Research Laboratory at New York University Langone Health) for his assistance with the slide preparation and pathological staining.

Source of Funding

This work was supported by funding from the National Institutes of Health R01-HL132073 and a Fondation Leducq Transatlantic Network of Excellence Award to DSP and R01-HL111314 to MKC and DVW, and the American Heart Association 20POST35080180 to NY.

Non-standard Abbreviations and Acronyms

AF	atrial fibrillation
AFL	atrial flutter
AngII	angiotensin II
ErbB4	Erb-B2 Receptor Tyrosine Kinase 4
ETV1	E twenty-six variant 1
HF	heart failure
HPS	His-Purkinje system
LA	left atrium

LVEF	left ventricular ejection fraction
NRG1	Neuregulin 1
NRVM	neonatal rat ventricular myocyte
RA	right atrium
TAC	transverse aortic constriction
TGFBR	transforming growth factor beta receptor
WT	wildtype

References

1. Dunlay SM and Roger VL. Understanding the epidemic of heart failure: past, present, and future. Curr Heart Fail Rep. 2014;11:404–415. doi: 10.1007/s11897-014-0220-x [PubMed: 25182014]
2. Jessup M, Abraham WT, Casey DE, Feldman AM, Francis GS, Ganiats TG, Konstam MA, Mancini DM, Rahko PS, Silver MA, et al.2009 focused update: ACCF/AHA Guidelines for the Diagnosis and Management of Heart Failure in Adults: a report of the American College of Cardiology Foundation/American Heart Association Task Force on Practice Guidelines: developed in collaboration with the International Society for Heart and Lung Transplantation. Circulation. 2009;119:1977–2016. doi:10.1161/CIRCULATIONAHA.109.192064 [PubMed: 19324967]
3. Gaspo R, Bosch RF, Bou-Abboud E and Nattel S. Tachycardia-induced changes in Na+ current in a chronic dog model of atrial fibrillation. Circ Res. 1997;81:1045–1052. doi:10.1161/01.res.81.6.1045 [PubMed: 9400386]
4. Gemel J, Levy AE, Simon AR, Bennett KB, Ai X, Akhter S and Beyer EC. Connexin40 abnormalities and atrial fibrillation in the human heart. J Mol Cell Cardiol. 2014;76:159–168. doi: 10.1016/j.yjmcc.2014.08.021 [PubMed: 25200600]
5. Gemel J, Simon AR, Patel D, Xu Q, Matiukas A, Veenstra RD and Beyer EC. Degradation of a connexin40 mutant linked to atrial fibrillation is accelerated. J Mol Cell Cardiol. 2014;74:330–339. doi: 10.1016/j.yjmcc.2014.06.010 [PubMed: 24973497]
6. Hanif W, Alex L, Su Y, Shinde AV, Russo I, Li N and Frangogiannis NG. Left atrial remodeling, hypertrophy, and fibrosis in mouse models of heart failure. Cardiovasc Pathol. 2017;30:27–37. doi:10.1016/j.carpath.2017.06.003 [PubMed: 28759817]
7. Shekhar A, Lin X, Lin B, Liu FY, Zhang J, Khodadadi-Jamayran A, Tsirigos A, Bu L, Fishman GI and Park DS. ETV1 activates a rapid conduction transcriptional program in rodent and human cardiomyocytes. Sci Rep. 2018;8:9944. doi:10.1038/s41598-018-28239-7 [PubMed: 29967479]
8. Shekhar A, Lin X, Liu FY, Zhang J, Mo H, Bastarache L, Denny JC, Cox NJ, Delmar M, Roden DM, et al.Transcription factor ETV1 is essential for rapid conduction in the heart. J Clin Invest. 2016;126:4444–4459. doi:10.1172/JCI87968 [PubMed: 27775552]
9. Wettschureck N, Rutten H, Zywietz A, Gehring D, Wilkie TM, Chen J, Chien KR and Offermanns S. Absence of pressure overload induced myocardial hypertrophy after conditional inactivation of Galphaq/Galpha11 in cardiomyocytes. Nat Med. 2001;7:1236–1240. doi:10.1038/nm1101-1236 [PubMed: 11689889]
10. Arber S, Ladle DR, Lin JH, Frank E and Jessell TM. ETS gene Er81 controls the formation of functional connections between group Ia sensory afferents and motor neurons. Cell. 2000;101:485–498. doi:10.1016/S0092-8674(00)80859-4 [PubMed: 10850491]
11. Daugherty A, Manning MW and Cassis LA. Angiotensin II promotes atherosclerotic lesions and aneurysms in apolipoprotein E-deficient mice. J Clin Invest. 2000;105:1605–1612. doi:10.1172/JCI7818 [PubMed: 10841519]
12. deAlmeida AC, van Oort RJ and Wehrens XH. Transverse aortic constriction in mice. J. Vis. Exp.2010; 38: e1729. doi:10.3791/1729

13. Hsu J, Gore-Panter S, Tchou G, Castel L, Lovano B, Moravec CS, Pettersson GB, Roselli EE, Gillinov AM, McCurry KR, et al.Genetic Control of Left Atrial Gene Expression Yields Insights into the Genetic Susceptibility for Atrial Fibrillation. Circ Genom Precis Med. 2018;11:e002107. doi:10.1161/CIRCGEN.118.002107 [PubMed: 29545482]
14. Rommel C, Rosner S, Lother A, Barg M, Schwaderer M, Gilsbach R, Bomicke T, Schnick T, Mayer S, Doll S, et al.The Transcription Factor ETV1 Induces Atrial Remodeling and Arrhythmia. Circ Res. 2018;123:550–563. doi: 10.1161/CIRCRESAHA.118.313036 [PubMed: 29930145]
15. Park DS, Cerrone M, Morley G, Vasquez C, Fowler S, Liu N, Bernstein SA, Liu FY, Zhang J, Rogers CS, et al.Genetically engineered SCN5A mutant pig hearts exhibit conduction defects and arrhythmias. J Clin Invest. 2015;125:403–412. doi: 10.1172/JCI76919 [PubMed: 25500882]
16. Chen KH, Xu XH, Sun HY, Du XL, Liu H, Yang L, Xiao GS, Wang Y, Jin MW and Li GR. Distinctive property and pharmacology of voltage-gated sodium current in rat atrial vs ventricular myocytes. Heart Rhythm. 2016;13:762–770. doi:10.1016/j.hrthm.2015.11.022 [PubMed: 26598320]
17. Hennessey JA, Marcou CA, Wang C, Wei EQ, Wang C, Tester DJ, Torchio M, Dagradi F, Crotti L, Schwartz PJ, et al.FGF12 is a candidate Brugada syndrome locus. Heart Rhythm. 2013;10:1886–1894. doi: 10.1016/j.hrthm.2013.09.064 [PubMed: 24096171]
18. Park DS, Shekhar A, Marra C, Lin X, Vasquez C, Solinas S, Kelley K, Morley G, Goldfarb M and Fishman GI. Fhf2 gene deletion causes temperature-sensitive cardiac conduction failure. Nat Commun. 2016;7:12966. doi:10.1038/ncomms12966 [PubMed: 27701382]
19. Park DS, Shekhar A, Santucci Iii J, Redel-Traub G, Solinas SM, Mintz S, Lin X, Chang EW, Narke D, Xia Y, Goldfarb M and Fishman GI. Ionic Mechanisms of Impulse Propagation Failure in the FHF2-Deficient Heart. Circ Res. 2020 9 23. doi: 10.1161/CIRCRESAHA.120.317349. Epub ahead of print
20. Denham NC, Pearman CM, Caldwell JL, Madders GWP, Eisner DA, Trafford AW and Dibb KM. Calcium in the Pathophysiology of Atrial Fibrillation and Heart Failure. Front Physiol. 2018;9:1380. doi:10.1161/CIRCEP.107.754788 [PubMed: 30337881]
21. Wang J, Li Z, Du J, Li J, Zhang Y, Liu J and Hou Y. The expression profile analysis of atrial mRNA in rats with atrial fibrillation: the role of IGF1 in atrial fibrosis. BMC cardiovascular disorders. 2019;19:40. doi:10.1186/s12872-019-1013-7 [PubMed: 30770724]
22. Vilahur G, Juan-Babot O, Pena E, Onate B, Casani L and Badimon L. Molecular and cellular mechanisms involved in cardiac remodeling after acute myocardial infarction. J Mol Cell Cardiol. 2011;50:522–533. doi:10.1016/j.yjmcc.2010.12.021 [PubMed: 21219908]
23. Liu G, Ma C, Yang H and Zhang PY. Transforming growth factor beta and its role in heart disease. Exp Ther Med. 2017;13:2123–2128. doi: 10.3892/etm.2017.4246 [PubMed: 28565818]
24. Verrecchia F, Chu ML and Mauviel A. Identification of novel TGF-beta /Smad gene targets in dermal fibroblasts using a combined cDNA microarray/promoter transactivation approach. J Biol Chem. 2001;276:17058–17062. doi:10.1074/jbc.M100754200 [PubMed: 11279127]
25. Allard MF, Schonekess BO, Henning SL, English DR and Lopaschuk GD. Contribution of oxidative metabolism and glycolysis to ATP production in hypertrophied hearts. Am J Physiol. 1994;267:H742–H750. doi:10.1152/ajpheart.1994.267.2.H742 [PubMed: 8067430]
26. Ritterhoff J, Young S, Villet O, Shao D, Neto FC, Bettcher LF, Hsu YA, Kolwicz SC, Jr., Raftery D and Tian R. Metabolic Remodeling Promotes Cardiac Hypertrophy by Directing Glucose to Aspartate Biosynthesis. Circ Res. 2020;126:182–196. doi:10.1161/CIRCRESAHA.119.315483 [PubMed: 31709908]
27. Chi P, Chen Y, Zhang L, Guo X, Wongvipat J, Shamu T, Fletcher JA, Dewell S, Maki RG, Zheng D, et al.ETV1 is a lineage survival factor that cooperates with KIT in gastrointestinal stromal tumours. Nature. 2010;467:849–853. doi:10.1038/nature09409 [PubMed: 20927104]
28. Cai C, Hsieh CL, Omwancha J, Zheng Z, Chen SY, Baert JL and Shemshedini L. ETV1 is a novel androgen receptor-regulated gene that mediates prostate cancer cell invasion. Mol Endocrinol. 2007;21:1835–1846. doi:10.1210/me.2006-0480 [PubMed: 17505060]
29. Gao G, Xiu D, Yang B, Sun D, Wei X, Ding Y, Ma Y and Wang Z. miR-129-5p inhibits prostate cancer proliferation via targeting ETV1. Onco Targets Ther. 2019;12:3531–3544. doi:10.2147/OTT.S183435 [PubMed: 31190859]

30. Mehra R, Dhanasekaran SM, Palanisamy N, Vats P, Cao X, Kim JH, Kim DS, Johnson T, Fullen DR and Chinnaiyan AM. Comprehensive Analysis of ETS Family Members in Melanoma by Fluorescence In Situ Hybridization Reveals Recurrent ETV1 Amplification. Transl Oncol. 2013;6:405–412. doi:10.1593/tlo.13340 [PubMed: 23908683]

31. Jorgensen R, Katta M, Wolfe J, Leach DF, Chun J and Wilsbacher LD. Deletion of Sphingosine 1-Phosphate Receptor 1 in cardiomyocytes during development leads to abnormal ventricular conduction and fibrosis. bioRxiv. Preprint posted online March 18, 2020. doi:10.1101/2020.03.15.993105

32. Sabir IN, Killeen MJ, Grace AA and Huang CL. Ventricular arrhythmogenesis: insights from murine models. Progress in biophysics and molecular biology. 2008;98:208–218. doi:10.1016/j.pbiomolbio.2008.10.011 [PubMed: 19041335]

33. Mitchell GF, Jeron A and Koren G. Measurement of heart rate and Q-T interval in the conscious mouse. Am J Physiol. 1998;274:H747–H751. doi:10.1152/ajpheart.1998.274.3.H747 [PubMed: 9530184]

34. Dobin A, Davis CA, Schlesinger F, Drenkow J, Zaleski C, Jha S, Batut P, Chaisson M and Gingeras TR. STAR: ultrafast universal RNA-seq aligner. Bioinformatics. 2013;29:15–21. doi:10.1093/bioinformatics/bts635 [PubMed: 23104886]

35. Anders S, Pyl PT and Huber W. HTSeq--a Python framework to work with high-throughput sequencing data. Bioinformatics. 2015;31:166–169. doi:10.1093/bioinformatics/btu638 [PubMed: 25260700]

36. Love MI, Huber W and Anders S. Moderated estimation of fold change and dispersion for RNA-seq data with DESeq2. Genome biology. 2014;15:550. doi:10.1186/s13059-014-0550-8 [PubMed: 25516281]

37. Quinlan AR and Hall IM. BEDTools: a flexible suite of utilities for comparing genomic features. Bioinformatics. 2010;26:841–842. doi:10.1093/bioinformatics/btq033 [PubMed: 20110278]

38. Yu G, Wang LG, Han Y and He QY. clusterProfiler: an R package for comparing biological themes among gene clusters. Omics : A Journal of Integrative Biology. 2012;16:284–287. doi:10.1089/omi.2011.0118 [PubMed: 22455463]

Clinical Perspective

What is New?

- This is the first demonstration that the left atrium (LA) undergoes remodeling in a highly conserved fashion using two murine models of cardiac pressure overload.
- Transcription factor ETV1 is downregulated in the LA in both cardiac pressure overload mouse models and in patients with reduced ejection fraction.
- Cardiomyocyte-selective *Etv1* deficient mice show downregulation of rapid conduction genes, reduced sodium current density, and upregulation of profibrotic gene programming, contributing to both electrical and structural remodeling in the LA.

What are the Clinical Implications?

- Our findings suggest that left atrial electrical and structural remodeling during cardiac pressure overload may be the result of downregulation of developmentally established transcriptional programs, such as ETV1.
- Our data identifies the ErbB4/ETV1 signaling pathway as a potential target for reverse atrial remodeling therapy in patients with reduced ejection fraction.

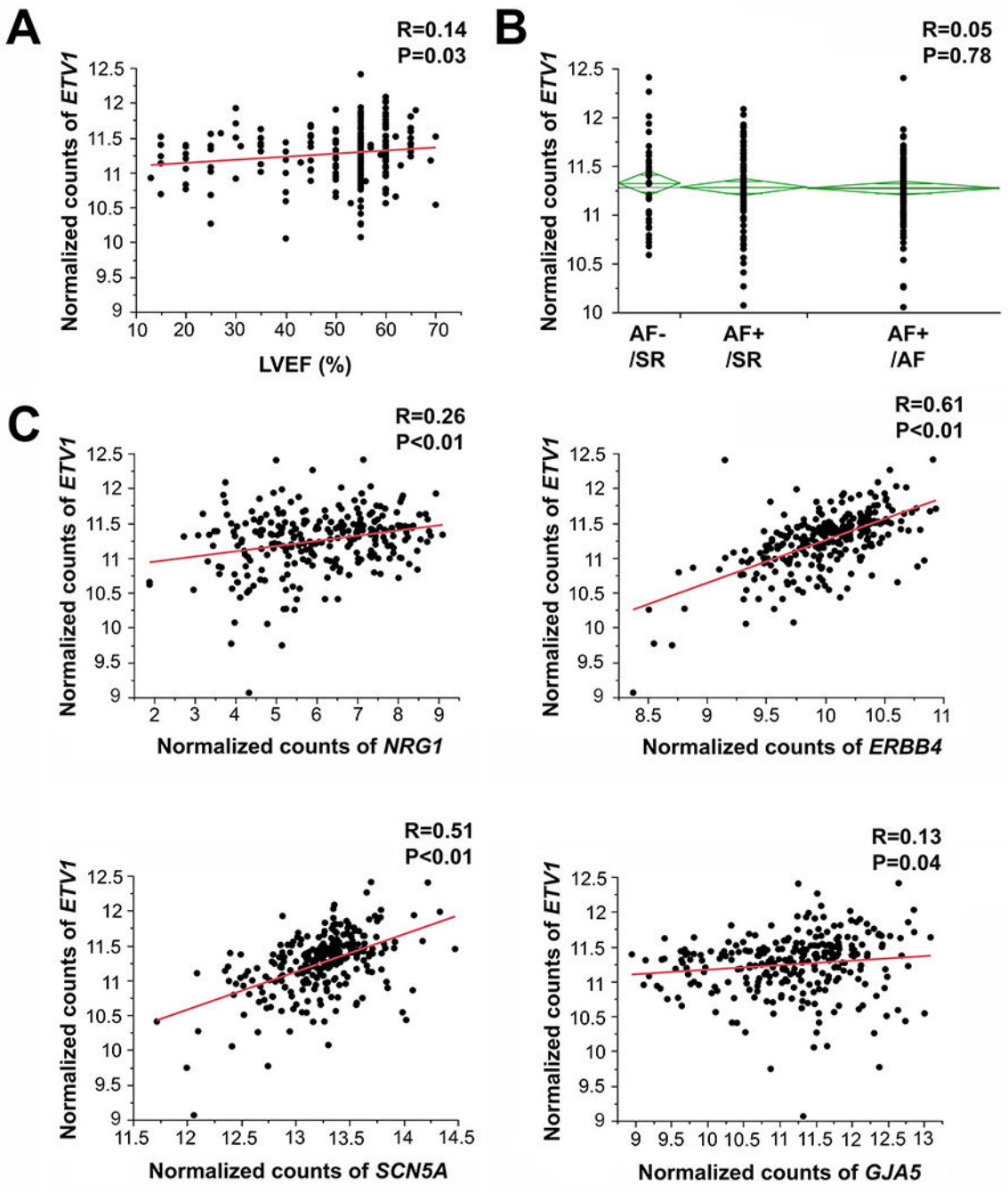

Figure 1. Transcription factor *ETV1* expression is reduced in patients with reduced ejection fraction.

(A–C)*ETV1* expression in the left atrium (LA) of 265 patients (251 patients who underwent heart surgery and 14 donors for heart transplant) correlates with left ventricular ejection fraction (LVEF) **(A)** but not with atrial fibrillation (AF) **(B).** Simple linear regression analysis or analysis of variance was used. AF-/SR: patients who had no history of AF and showed sinus rhythm (SR) at the time of surgery, AF+/SR: patients diagnosed with AF who were in SR at time of surgery, AF+/AF: patients diagnosed with AF and were

in AF or atrial flutter at time of surgery. **(C)** *ETV1* expression correlates with the NRG1/ERBB4 signaling pathway and rapid conduction genes, *SCN5A and GJA5*, by simple linear regression analysis.

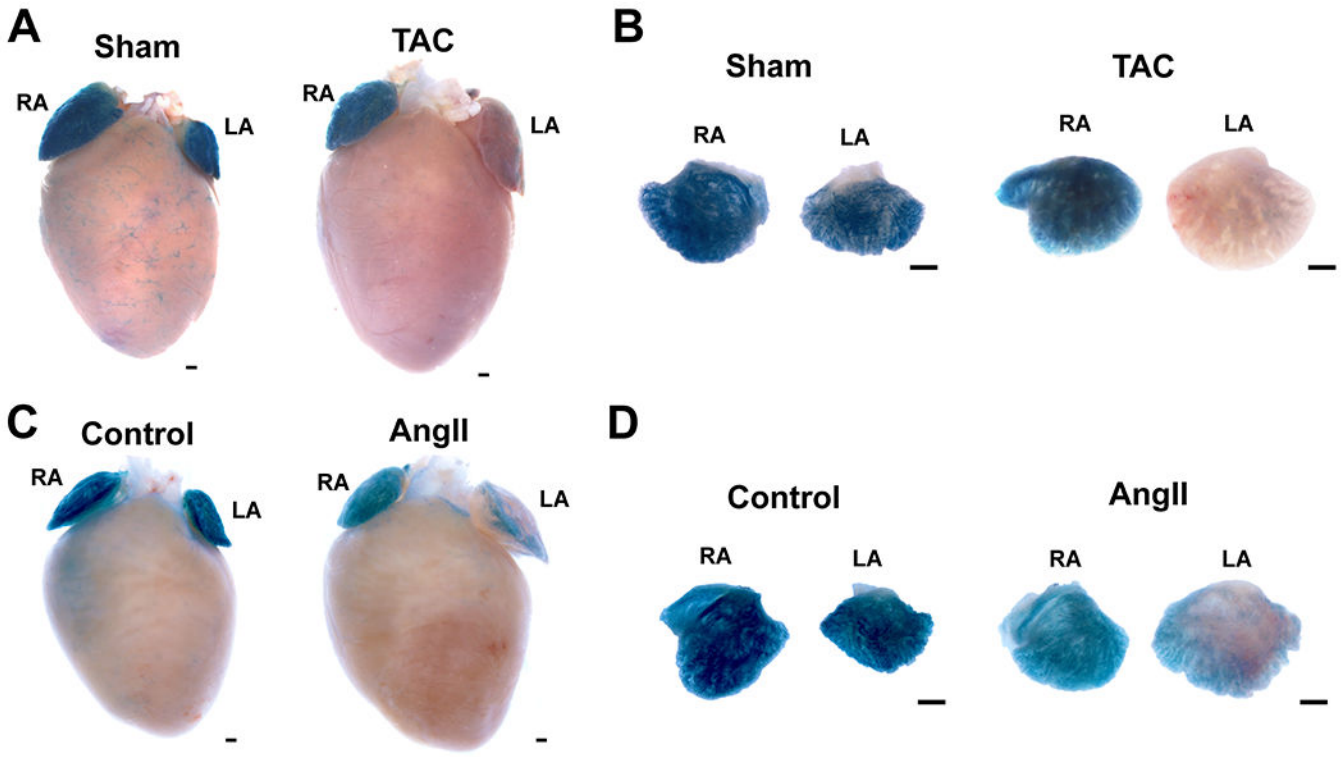

Figure 2. Cardiac pressure overload reduces *Etv1-nlz* reporter gene expression in the left atrium.

(**A–D)** *Etv1* expression in the $Etv1^{nlz/+}$ reporter mouse is reduced in the left atrium (LA) after 2 weeks of transverse aortic constriction (TAC) banding **(A, B)** or 2 weeks of angiotensin II (AngII) treatment **(C, D)** compared to control. Etv1-nlz reporter gene expression is minimally affected in the right atrium (RA) in TAC banded hearts. AngII treatment showed reduced expression of *Etv1-nlz* reporter gene expression in the RA but to a lesser extent than in the LA. Scale bars 500 μm in (A, C), 1 mm in (B, D).

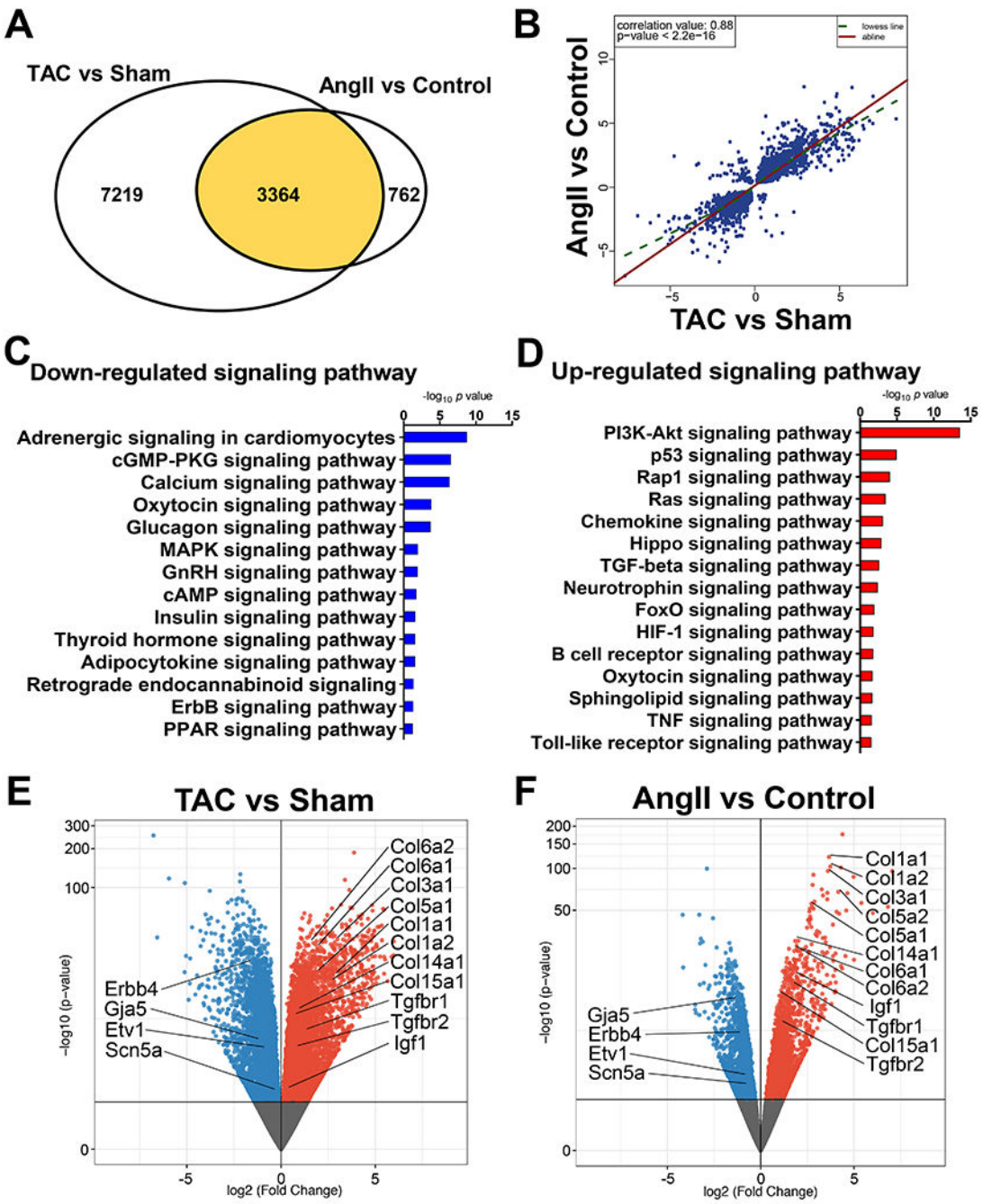

Figure 3. RNA-seq analysis shows differentially expressed genes in the mouse left atrium (LA) with transverse aortic constriction (TAC) banding and Angiotensin II (AngII) infusion.

(A) Venn diagram displaying overlap of 3364 differentially expressed genes between TAC and AngII[14] experiments. **(B)** Pairwise correlation between log fold change of differential gene expression in AngII vs. TAC banded experiments ($R = 0.88$, $P < 2.2\times10^{-16}$). **(C, D)** KEGG pathway analysis of the downregulated (C) and upregulated (D) genes involved in signaling pathways from the group of 3364 overlapping genes in (A). **(E, F)** Volcano plots of differential expression in the LA from TAC banded **(E)** and AngII infused **(F)** mice.

All significant differentially expressed genes ($P < 0.05$) are labeled blue (downregulated) or red (upregulated) and all non-significant differentially expressed genes are labeled in gray. Downregulation of *Etv1, Erbb4, Scn5a*, and *Gja5* and upregulation of pro-fibrotic genes (*Tgfbr1, Tgfbr2, Igf1*, and numerous collagen genes) are similar between TAC banding and AngII infusion.

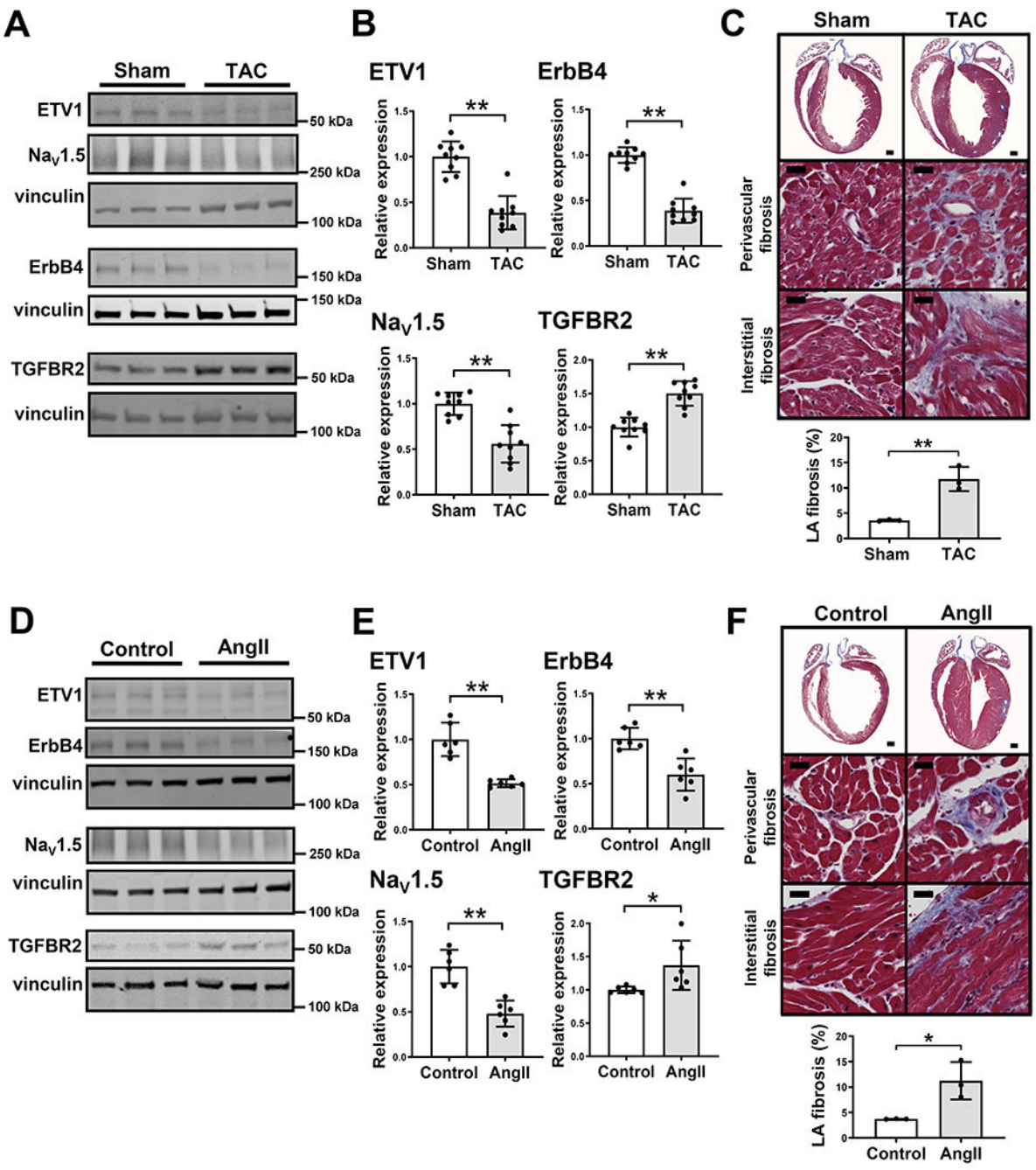

Figure 4. TAC banding and AngII treatment reduced ETV1, ErbB4, and Na$_V$1.5, and increased fibrosis in the left atria.

Quantitative values were normalized to vinculin. Values show mean±SD. Student's *t*-test was used for statistical analysis except Mann–Whitney test for ETV1 expression for TAC vs. sham. *P < 0.05, **P < 0.01. n = 6–9 per group. **(A, B)** In the left atrium (LA), ETV1, ErbB4, and Na$_V$1.5 are reduced, while TGFBR2 is increased in transverse aortic constriction (TAC) banded mice compared to sham-operated mice. Molecular weight on western blot: ETV1 ~58 kDa, ErbB4 ~180 kDa, Na$_V$1.5 ~260 kDa, TGFBR2 ~55 kDa, and vinculin ~125

kDa. **(C)** Masson's trichrome staining displays fibrotic changes in the LA in TAC banded mice. Whole LA section was analyzed for fibrosis area using ImageJ. Values are shown as mean±SD. **P < 0.01 by Student's *t*-test. n = 3 per group. Scale bars 500μm for top, 20μm for middle and bottom. **(D, E)** In the LA, ETV1, ErbB4, and $Na_V1.5$ are reduced, while TGFBR2 is increased in angiotensin II (AngII) infused mice compared to vehicle control treated mice. Molecular weight on western blot: ETV1 ~58 kDa, ErbB4 ~180 kDa, $Na_V1.5$ ~260 kDa, TGFBR2 ~55 kDa, and vinculin ~125 kDa. **(F)** Masson's trichrome staining displays fibrotic changes in the LA in AngII treated mice. Whole LA section was analyzed for fibrosis area using ImageJ. Values are shown as mean±SD. *P < 0.05 by Student's *t*-test. n = 3 per group. Scale bars 500μm for top, 20μm for middle and bottom.

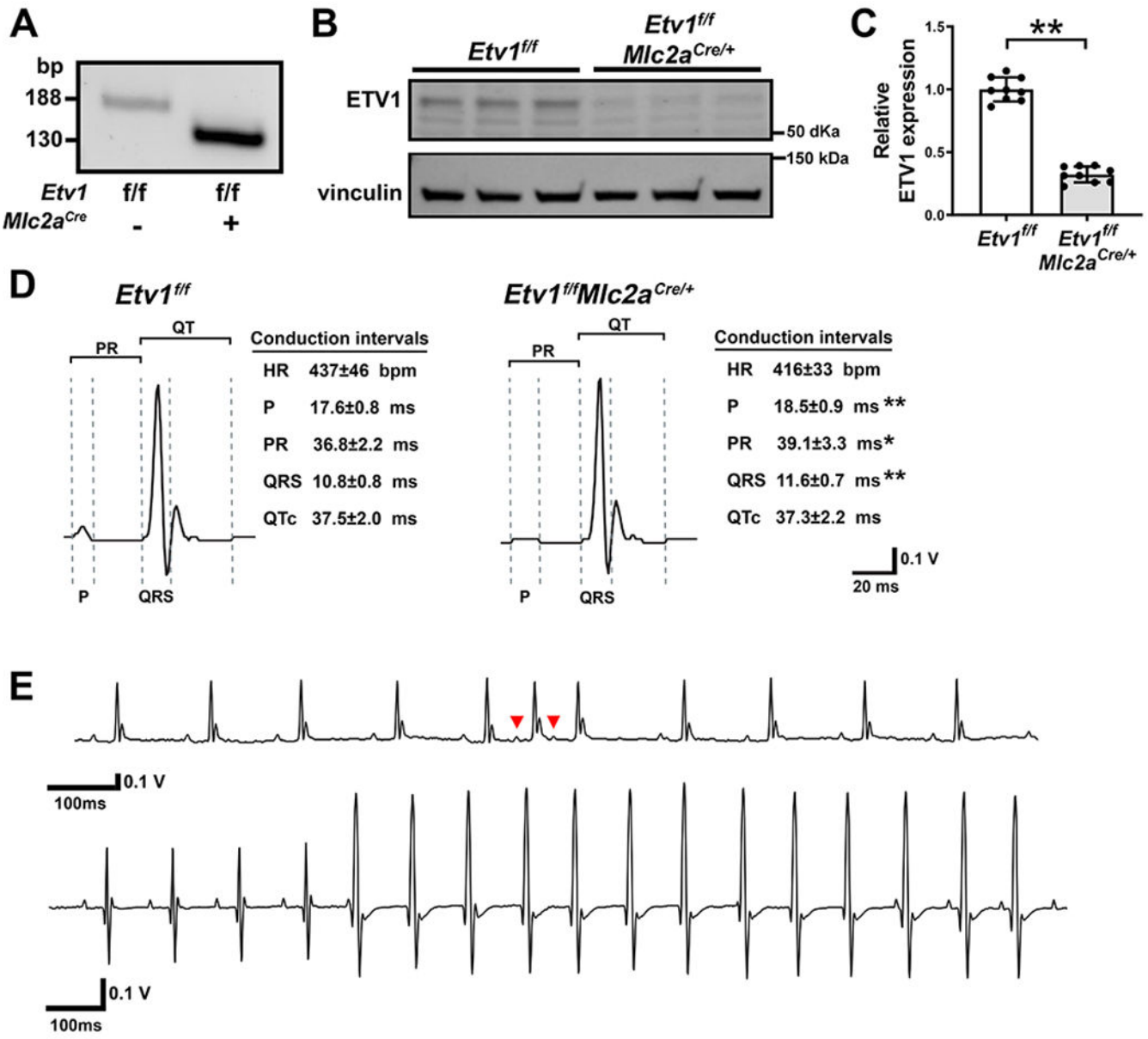

Figure 5. *Etv1* knockout (*Etv1*$^{f/f}$*Mlc2a*$^{Cre/+}$) model demonstrates cardiac conduction disturbance and arrhythmia.

(A) PCR analysis of DNA from left atrial tissue displaying targeted *Etv1* exon 11 deletion in the left atrium (LA) of *Etv1*$^{f/f}$*Mlc2a*$^{Cre/+}$ mice. The 188 and 130 bp bands represent unrecombined and recombined f/f alleles, respectively. **(B, C)** Western blot assay and densitometric analysis showing reduced ETV1 expression in the LA in *Etv1*$^{f/f}$*Mlc2a*$^{Cre/+}$ mice. Molecular weight on western blot: ETV1 ~58 kDa and vinculin ~125 kDa. Values are presented as mean±SD. **P < 0.01 by Student's *t*-test. **(D)** Representative electrocardiogram (ECG) traces recorded from sedated *Etv1*$^{f/f}$*Mlc2a*$^{Cre/+}$ and control (*Etv1*$^{f/f}$) mice. ECG parameters analyzed with LabChart v8.1.9 demonstrate prolonged P duration, PR interval, and QRS interval in *Etv1*$^{f/f}$*Mlc2a*$^{Cre/+}$ mice (n = 13) compared to control (n = 17). Values are presented as mean±SD. *P < 0.05, **P < 0.01 by Student's *t*-test. HR, heart rate; QTc,

corrected QT interval. **(E)** Representative ECG traces in *Etv1*$^{f/f}$*Mlc2a*$^{Cre/+}$ mice showing abnormalities. Upper trace indicates atrial ectopic beats (red arrowhead), and lower trace indicates non-sustained ventricular tachycardia.

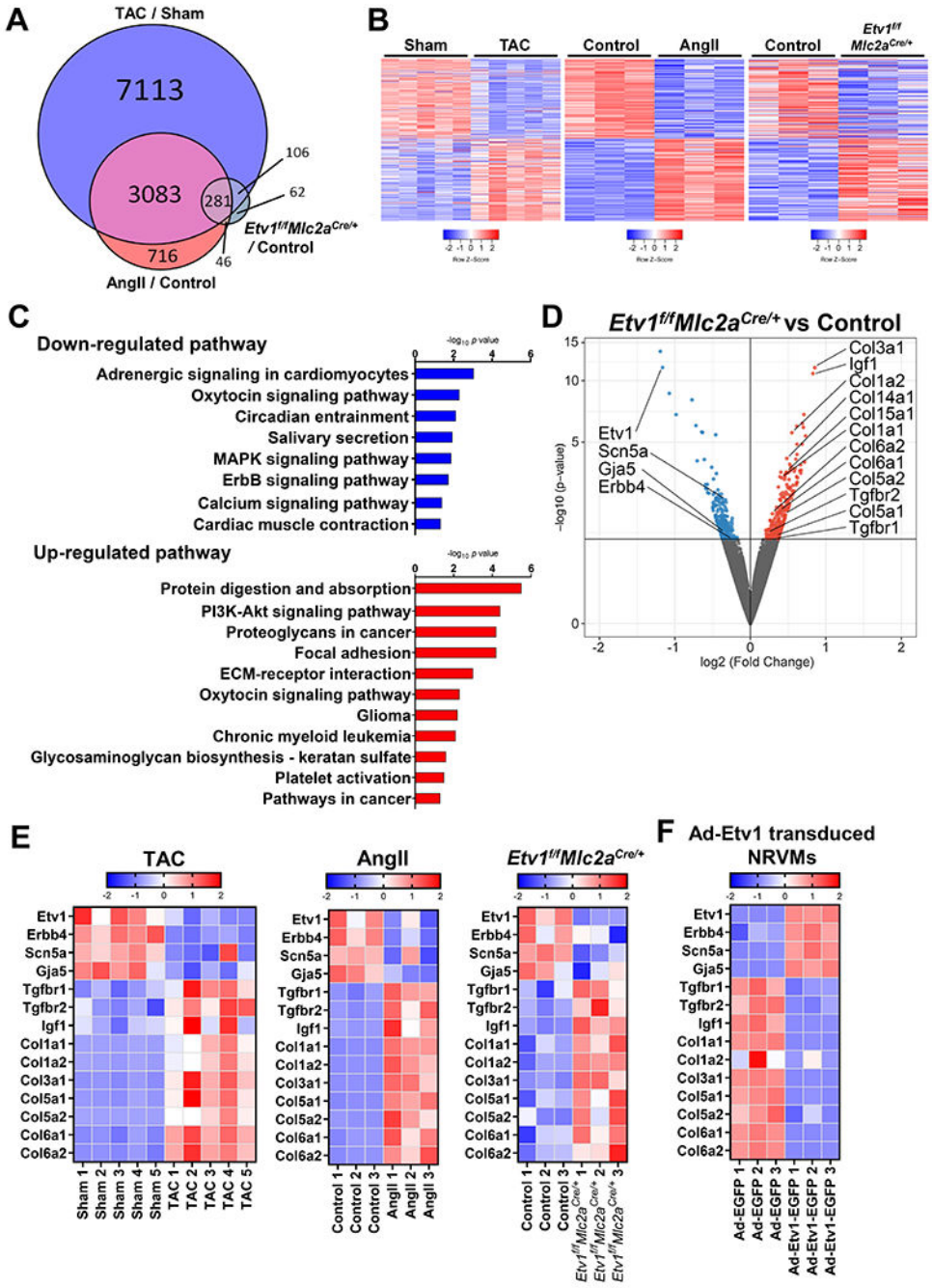

Figure 6. Comparison of gene expression between *Etv1* loss-of-function, *Etv1* gain-of-function, TAC banded, and AngII treated models.

(A) Venn diagram of differentially expressed genes in the left atrium from three model systems, transverse aortic constriction (TAC) banded, angiotensin II (AngII) treated, and *Etv1*$^{f/f}$*Mlc2a*$^{Cre/+}$ models, reveals 281 overlapping genes. **(B)** Heatmap of the 281 overlapping genes from (A) show highly similar expression patterns between TAC banded, AngII treated, and *Etv1*$^{f/f}$*Mlc2a*$^{Cre/+}$ models. **(C)** KEGG pathway analysis of the 281 overlapping genes separated into downregulated (blue) and upregulated (red) groups (18

non-redundant categories are shown). **(D)** Volcano plot of differential expression from *Etv1*$^{f/f}$*Mlc2a*$^{Cre/+}$ shows down-regulation of *Erbb4, Scn5a* and *Gja5* and up-regulation of pro-fibrotic genes (*Tgfbr1, Tgfbr2, Igf1*, and collagen genes) as similarly seen in pressure overload models. All significant differentially expressed genes ($P < 0.05$) are labeled blue (down-regulated) or red (up-regulated) and all non-significant differentially expressed genes are labeled in gray. **(E)** Heatmap showing similar gene expression profiles of *Etv1, Erbb4, Scn5a, Gja5* and pro-fibrotic genes in the three model systems. **(F)** Heat map from neonatal rat ventricular myocytes (NRVMs) transduced with Ad-Etv1-EGFP (normalized to Ad-EGFP) demonstrates that adenoviral mediated expression of *Etv1* in NRVMs causes reciprocal changes in gene expression compared to TAC banded, AngII treated, and *Etv1*$^{f/f}$*Mlc2a*$^{Cre/+}$ models.

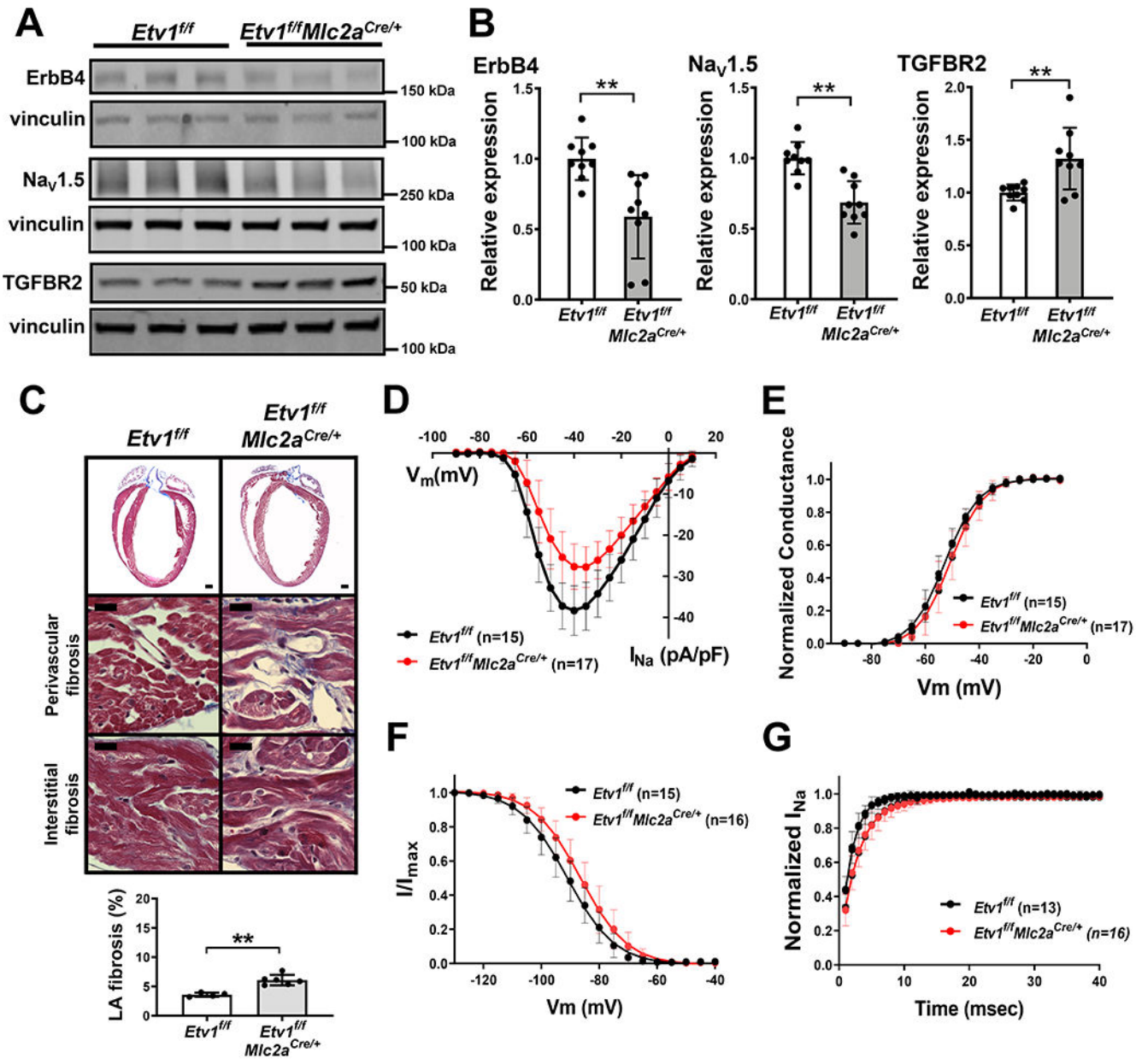

Figure 7. Protein level and functional characterization of the left atrium (LA) from *Etv1* knockout (*Etv1*$^{f/f}$*Mlc2a*$^{Cre/+}$) mice.

(A) Representative immunoblots of ErbB4, $Na_V1.5$, and TGFBR2 in *Etv1*$^{f/f}$*Mlc2a*$^{Cre/+}$ vs. littermate control (*Etv1*$^{f/f}$) mice. Molecular weight on western blot: ErbB4 ~180 kDa, $Na_V1.5$ ~260 kDa, TGFBR2 ~55 kDa, and vinculin ~125 kDa. **(B)** Densitometric measurements normalized to vinculin show ErbB4 and $Na_V1.5$ are reduced, while TGFBR2 is increased in the LA in *Etv1*$^{f/f}$*Mlc2a*$^{Cre/+}$ compared to *Etv1*$^{f/f}$ mice (n = 9 per group). Values are presented as mean±SD. **P < 0.01 by Student's *t*-test. **(C)** Masson's trichrome staining displays fibrotic changes in the LA in *Etv1*$^{f/f}$*Mlc2a*$^{Cre/+}$ *mice* at 16–20 weeks old. Whole LA section was analyzed for fibrosis area using ImageJ. Values are shown as mean±SD. **P < 0.01 by Student's *t*-test. n = 4–6 per group. Scale bars 500μm for top,

20μm for middle and bottom. **(D–G)** Whole-cell patch clamp data from dissociated left atrial myocytes using *Etv1*$^{f/f}$*Mlc2a*$^{Cre/+}$ and control (*Etv1*$^{f/f}$) mice. **(D)** I-V relationship curve of sodium currents recorded from *Etv1*$^{f/f}$*Mlc2a*$^{Cre/+}$ (n = 17/3 cells/mice) and control (n = 15/3 cells/mice) left atrial cardiomyocytes. The amplitudes of sodium current were normalized to cell capacitance and presented as mean±SD. **(E)** Voltage dependence of the normalized conductance of I_{Na}. (n = 17/3 cells/mice for *Etv1*$^{f/f}$*Mlc2a*$^{Cre/+}$ and n = 15/3 cells/mice for control). **(F)** Voltage dependence of steady-state inactivation (n = 16/3 cells/mice for *Etv1*$^{f/f}$*Mlc2a*$^{Cre/+}$ and n = 15/3 cells/mice for control) **(G)** Time course of recovery from inactivation. (n = 16/3 cells/mice for *Etv1*$^{f/f}$*Mlc2a*$^{Cre/+}$ and n = 13/3 cells/mice for control).

Table 1.

Demographic and clinical characteristics of 265 human subjects

Whole Cohort (Surgical and Donor, n=265)	
Age, years	60±12 (18–86)
Sex	
Male	181 (68)
Female	84 (32)
Race	
White	188 (71)
Black	77 (29)
Surgical Cohort (n=251)	
Age, years	61±12 (21–86)
Sex	
Male	175 (70)
Female	76 (30)
Race	
White	222 (88)
Black	29 (12)
BMI, kg/m^2	28±6 (18–49)
Type of atrial fibrillation	213 (85)
Paroxysmal	58 (27)
Persistent	40 (19)
Permanent	104 (49)
Presence of Comorbidities	
NYHA Functional Classification	
I	67 (26)
II	128 (51)
III	53 (21)
IV	3 (1)
Hypertension	138 (55)
Diabetes	178 (71)
Myocardial Infarction	51 (20)
Smoking	124 (49)
Peripheral Vascular Disease	57 (23)
Chronic Obstructive Pulmonary Disease	41 (16)
Renal Disease	3 (1)
Thyroid Disease	39 (16)
- Hyper	5 (13)
- Hypo	34 (87)
Echocardiogram findings	
LVEF, %	51±12 (13–70)

Whole Cohort (Surgical and Donor, n=265)	
LA size, mm	49±9 (29–75)
RVSP, mmHg	38±13 (9–99)
Medication use	
Antiarrhythmics	76 (31)
Amiodarone	30 (39)
ACE-I/ARB	131 (52)
Beta-blocker	144 (57)

Values are shown as mean±SD (range) or n (%). BMI, Body Mass Index; NYHA, New York Heart Association; LVEF, Left Ventricular Ejection Fraction; LA, Left Atrium; RVSP, Right Ventricular Systolic Pressure; ACE-I, Angiotensin Converting Enzyme Inhibitor; ARB, Angiotensin II Receptor Blocker.